Title
Projected changes in early summer ridging and drought over the Central Plains

Journal
Environmental Research Letters, 17(10)

ISSN
1748-9318

Authors
Cook, Benjamin I
Williams, A Park
Marvel, Kate

Publication Date
2022-10-01

DOI
10.1088/1748-9326/ac8e1a

Peer reviewed

ENVIRONMENTAL RESEARCH
LETTERS

LETTER • OPEN ACCESS

Projected changes in early summer ridging and drought over the Central Plains

To cite this article: Benjamin I Cook *et al* 2022 *Environ. Res. Lett.* **17** 104020

ENVIRONMENTAL RESEARCH
LETTERS

OPEN ACCESS

RECEIVED
8 June 2022

REVISED
3 August 2022

ACCEPTED FOR PUBLICATION
31 August 2022

PUBLISHED
23 September 2022

LETTER

Projected changes in early summer ridging and drought over the Central Plains

Benjamin I Cook[1,2,*], **A Park Williams**[3] **and Kate Marvel**[1]

[1] NASA Goddard Institute for Space Studies, 2880 Broadway, New York, NY 10025, United States of America
[2] Lamont-Doherty Earth Observatory, Palisades, New York, NY 10964, United States of America
[3] University of California, Los Angeles, Los Angeles, CA 90095, United States of America
[*] Author to whom any correspondence should be addressed.

E-mail: benjamin.i.cook@nasa.gov

Keywords: drought, central plains, atmospheric ridging, paleoclimate, tree-rings, CMIP6

Supplementary material for this article is available online

Abstract

Early summer (May–June–July; MJJ) droughts over the Central Plains are often caused by atmospheric ridging, but it is uncertain if these events will increase in frequency or if their influence on drought severity will change in a warming world. Here, we use tree-ring based reconstructions (1500–2020 CE) of MJJ ridging and 0–200 cm soil moisture with six CMIP6 model ensembles to investigate the response of Central Plains drought dynamics to a moderate warming scenario (SSP2-4.5). By the end of the 21st century (2071–2100), precipitation increases in most models during the preceding months (February–March–April), especially over the northern part of the Central Plains, while changes during MJJ are non-robust. By contrast, vapor pressure deficit increases strongly in all models, resulting in five of the six models projecting robust median soil moisture drying and all six models projecting more rapid seasonal soil moisture declines during the transition into the summer. Major ridging events increase in frequency in some models, and there is strong agreement across all models that when ridging events do occur, they will cause more severe soil moisture drought and seasonal drying at the end of the 21st century. The median multi-model response also indicates, by the end of the 21st century, that the Central Plains will experience a three-fold increase in the risk of drought events equivalent to the most extreme droughts of the last 500 years. Our results demonstrate that even moderate warming is likely to increase early summer soil moisture drought severity and risk over the Central Plains, even in the absence of robust precipitation declines, and that drought responses to major atmospheric ridging events will be significantly stronger.

1. Introduction

Warm season droughts are a major environmental hazard in the Central Plains of the United States (Schubert *et al* 2004a, Basara *et al* 2013), with especially severe events occurring in 1956 (Logan *et al* 2010), 1988 (Trenberth *et al* 1988), 2006 (Dong *et al* 2011), 2012 (Hoerling *et al* 2014, Otkin *et al* 2016), and during the 'Dust Bowl' of the 1930s (Schubert *et al* 2004b). Central Plains droughts are typically linked to persistent atmospheric ridges that cause strong subsidence and suppress precipitation in the region (Cook *et al* 2014, Wang *et al* 2015, Basara *et al* 2019, Jong *et al* 2022) and are amplified by land-atmosphere interactions that can enhance extreme heat (Dong *et al* 2011, Cowan *et al* 2020) and precipitation deficits (Schubert *et al* 2004a, Cook *et al* 2009). The Central Plains region is also prone to quickly developing 'flash drought' events (Otkin *et al* 2018, Pendergrass *et al* 2020, Jong *et al* 2022), characterized by rapid declines in soil moisture triggered by large precipitation deficits and high temperatures (Hobbins *et al* 2016, Pendergrass *et al* 2020).

Compared to regions with more robust drought responses to warming (e.g. southwestern North America, the Mediterranean) (Cook *et al* 2020), projected changes in Central Plains drought in twenty-first century warming scenarios are relatively

uncertain. Within the latest suite of climate model projections (Phase 6 of the Coupled Model Intercomparison Project (CMIP6)) (Eyring *et al* 2016), there is little change in annual precipitation over the Central Plains (Cook *et al* 2020, Ukkola *et al* 2020), but a strong and robust shift in precipitation seasonality, characterized by large increases during the cold season and modest declines during the warm season (Marvel *et al* 2021). Despite these complex and uncertain precipitation responses, however, some studies have found that warm season soil moisture drought risk and severity in the region will likely increase as a consequence of warming-induced increases in evaporative demand (Cook *et al* 2015, 2020, Marvel *et al* 2021, Ting *et al* 2021). There is also some evidence that the atmospheric circulation events that drive many seasonal droughts will increase in frequency and persistence with warming in the mid-latitudes (Coumou *et al* 2018, Kornhuber and Tamarin-Brodsky 2021, Sun *et al* 2022), where the Central Plains is located.

To date, however, projected changes in Central Plains drought, and the related circulation patterns (atmospheric ridges), have not been investigated in detail in CMIP6. In this study, we use a suite of CMIP6 model ensembles and a recent reconstruction of soil moisture and atmospheric ridging (Bolles *et al* 2021) to analyze projected changes in early summer (May–June–July; MJJ) Central Plains drought dynamics. These reconstructions cover the past 500 years (1500–2020 CE), providing new estimates of the long-term relationship between atmospheric ridging and soil moisture drought in the region and a multi-centennial dataset against which the model simulations can be evaluated. We specifically address the following research questions: (a) how robust are twenty-first century Central Plains drought responses (precipitation, soil moisture, vapor pressure deficit) within and across models?; (b) does the occurrence of ridging conditions associated with drought in the region significantly change with warming?; (c) how does the relationship between ridging and precipitation or soil moisture deficits shift in a warmer world?

2. Methods

2.1. Soil moisture and ridging index reconstructions

The soil moisture and ridging indices, and their tree-ring based reconstructions, were developed by Bolles *et al* (2021). The soil moisture index uses 0–200 cm soil moisture averaged over the Central Plains (32–47° N, 105–95° W), derived from observationally forced land surface model simulations of the twentieth century. The ridge index is a composite of regional averaged 600 hPa geopotential heights (32.5–42.5° N, 107.5–92.5° W), 700–500 hPa zonal winds (42.5–47.5° N, 115.5–87.5° W; 25–32.5° N, 110–87.5° W), and 700–500 hPa meridional winds (32.5–52.5° N, 120–110° W; 32.5–52.5° N, 90–77.5° W). These variables and regions used to construct the ridge index were selected based on empirical relationships between atmospheric circulation and soil moisture conditions in the central United States (Bolles *et al* 2021). Positive values of the ridge index indicate anomalous ridge conditions, typically associated with precipitation and soil moisture drought over the Central Plains, while negative values indicate anomalous trough conditions. Reconstructions of each index, spanning 1500–1983 CE, were developed using two completely independent networks of tree-ring chronologies from the central United States. These reconstructions where then merged with observations to cover a total of 521 years (1500–2020 CE). Further details on construction of the indices and the tree-ring reconstructions can be found in (Bolles *et al* 2021), and these data can be freely downloaded from www.dropbox.com/s/yv3hbioaid0bcko/reconstructions_stand.csv.

For our analyses, we standardized both indices to a mean of zero and unit standard deviation using a baseline period of 1851–1950, a century-long interval prior to the onset of accelerated warming that begins in the latter half of the 20th century. The correlation (Pearson's r, 1500–2020) between the two indices is −0.50, and both show pronounced interannual (thin lines) and decadal (thick lines) variability over the last five centuries (figure 1, top and middle panels). The two driest soil moisture values are 1934 (-2.33σ) and 1956 (-2.22σ), years occurring during the decadal-scale Dust Bowl (Schubert *et al* 2004b, Cook *et al* 2014) and 1950s (Palmer and Seamon 1957, Heim 2017) droughts, respectively. Both of these drought years were associated with anomalously strong ridging ($+1.45\sigma$ for 1934; $+2.37\sigma$ for 1956), with 1956 standing out as the fourth highest ridge index value in the record. The influence of ridging events on soil moisture is also demonstrated when soil moisture is compared during major ridge and trough events (figure 1, bottom panel). Ridge and trough events are defined as years where the ridge index falls within the upper or lower quartiles, respectively, with these thresholds determined using the 1851–1950 baseline. During major ridge events ($n = 105$), median soil moisture is -0.56σ, while during trough events median soil moisture is $+0.53\sigma$ ($n = 95$).

2.2. CMIP6 model projections

For our CMIP6 analyses, we used output from continuous ensemble members (1850–2100) using the *historical* and *SSP2-4.5* scenarios (table 1). The historical simulations use estimated natural (e.g. solar, volcanic) and anthropogenic (e.g. greenhouse gases, land use, aerosols) forcings to simulate the historical climate evolution from 1850 to 2014. SSP2-4.5

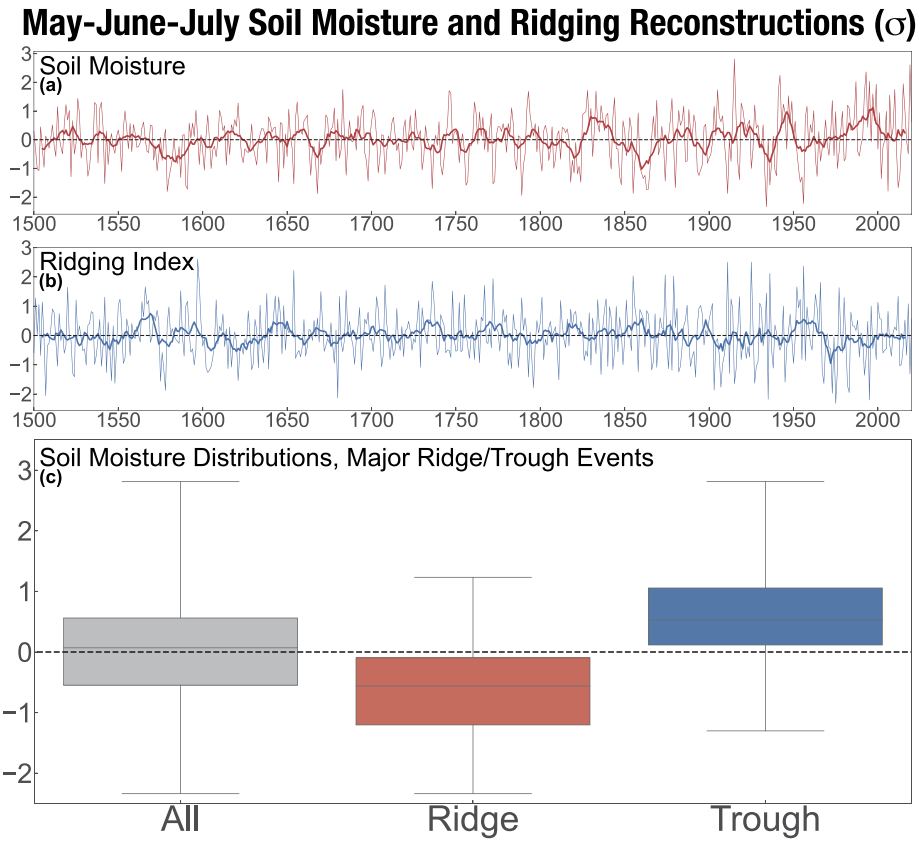

Figure 1. Empirical indices (tree-ring based reconstructions and observations) of May–June–July (MJJ) soil moisture (top panel) and ridging (middle panel) from 1500 to 2020. Both time series are standardized to a zero mean and unit standard deviation using a baseline period of 1851–1950. Box and whisker plots (bottom panel) show distributions of soil moisture for all years ($n = 521$), ridge events ($n = 105$, defined as years where the ridge index falls within the upper quartile using the 1851–1950 baseline period), and trough events ($n = 95$, defined as years where the ridge index falls within the lower quartile using the 1851–1950 baseline period). Thin lines are the inter-annual time series, while decadal variability is highlighted using a ten year moving average (thick lines).

Table 1. Continuous (historical+SSP2-4.5, 1851–2100) CMIP6 models and ensemble members used in the present study. Table includes the model name; the number of ensemble members used; the estimated equilibrium climate sensitivity (ECS, K) taken from Meehl *et al* (2020); the DOI references associated with these model submissions to CMIP6; and the names of the individual ensemble members. All CMIP6 data used in this study are available from the Earth System Grid (https://esgf-node.llnl.gov/search/cmip6/).

Model	#Ens.	ECS	DOI	Member names
ACCESS-ESM1-5	9	3.9	Ziehn *et al* (2019a) Ziehn *et al* (2019b)	r[1-6]i1p1f1, r[8-10]i1p1f1
CanESM5	48	5.6	Swart *et al* (2019a) Swart *et al* (2019b)	r[1-25]i1p2f1, r[1-13]i1p1f1 r[15]i1p1f1, r[17-25]i1p1f1
EC-Earth3	12	4.3	EC-Earth Consortium (2019a) EC-Earth Consortium (2019b)	r[1-2]i1p1f1, r7i1p1f1, r[9-11]i1p1f1, r13i1p1f1, r[15-17]i1p1f1, r[21-22]i1p1f1
GISS-E2-1-G	9	2.7	NASA GISS (2018) NASA GISS (2020)	r[1-5]i1p3f1, r[1-4]i1p5f1
IPSL-CM6A-LR	11	4.6	Boucher *et al* (2018) Boucher *et al* (2019)	r[1-6]i1p1f1, r[10-11]i1p1f1, r14i1p1f1, r22i1p1f1, r25i1p1f1
MPI-ESM1-2-LR	10	3.0	Wieners *et al* (2019a) Wieners *et al* (2019b)	r[1-10]i1p1f1

is a moderate warming and forcing scenario for the twenty-first century (2015–2100), designed to generate a top of the atmosphere radiative imbalance of $+4.5\ \mathrm{W\ m^{-2}}$ by 2100. We chose SSP2-4.5 specifically because it is considered a moderate or 'middle-of-the-road' warming and forcing scenario, and also stabilizes in time during the latter half of the twenty-first century.

Beyond changes in the mean state, we are also interested in precipitation and soil moisture responses associated with ridge and trough events. We therefore limited our analyses to models where we could access all the necessary variables for our calculations (see next paragraph) from a substantial number of ensemble members to increase event sampling. Using these criteria, we identified six models (table 1) with the number of available ensemble members ranging from 9 (ACCESS-ESM1-5, GISS-E2-1-G) to 48 (CanESM5). With the exception of CanESM5, equilibrium climate sensitivity for all models falls within the 5th%–95th% 'very likely' confidence range of 2.3–4.7 K, as estimated from a recent assessment (Sherwood *et al* 2020), although three models fall out of the assessed 'likely' range (2.6–3.9 K). Average warming across all six models for 2071–2100 is 3.0 K above preindustrial, slightly higher than the observationally constrained 2.6 K assessed warming for the SSP2-4.5 scenario from the Sixth Assessment Report (AR6) of the Intergovernmental Panel on Climate Change (IPCC) (Hausfather *et al* 2022).

To compare against our empirical indices, we calculated the same ridging and soil moisture indices from the models using the same methodology as Bolles *et al* (2021). For the ridging index, we used variables ua (*eastward wind*), va (*northward wind*), and zg (*geopotential height*). Prior to calculating the ridge index, thermal dilation effects in the geopotential height fields were removed by subtracting the ensemble mean of the zonal average geopotential height from the same latitudes. The soil moisture index was calculated using mrsol (*total water content of each soil layer*), which we integrated from the surface to 200 cm to match the reconstructed index. We then averaged our derived 0–200 cm soil moisture index over MJJ and the Central Plains.

We also analyzed changes in pr (*precipitation flux, including both liquid and solid phases*) and vapor pressure deficit, which we calculated using hurs (*near surface relative humidity*) and tas (*near surface air temperature*) with the August–Roche–Magnus formula (equation (6), Lawrence (2005)). Finally, we calculated an April–July soil drying index, also analyzed in Bolles *et al* (2021), that reflects the rate at which soil moisture decreases during the transition from the main seasons of moisture supply (winter and spring) to the season of highest moisture demand (summer). While not specifically a drought indicator, the drying index quantifies how quickly Central Plains soil moisture changes during the transition from spring to summer, when water demand, moisture stress, and heat stress are all likely to reach their seasonal peaks. If, with warming, this seasonal soil moisture dry-down does accelerate, it would likely translate to increased moisture stress on ecosystems and agriculture in the region, even absent any large mean state shifts in soil moisture. The drying index is calculated by first subtracting 0–200 cm July soil moisture from 0 to 200 cm April soil moisture, and then regressing out the effect of April soil moisture on this difference. Positive values of the drying index indicate faster than average seasonal dry down conditions.

All regional average variables and model indices (ridging, soil moisture, drying) were standardized to the same baseline as the reconstructions (1851–1950). Analyses of changes over time compare 2071–2100 against the baseline period (1851–1950) or latter part of the historical simulation (1985–2014). To assess spatially explicit differences in each model ensemble, we use the robustness metric (R) from Knutti and Sedlacek (2013), which uses information on the magnitude and sign of the ensemble mean change, as well as variability within and across the ensemble members. The upper bound is $R = 1.0$, which indicates perfect agreement across all ensemble members, and we use a threshold of $R \geqslant 0.80$ for determining robustness, which Knutti and Sedlacek (2013) considered 'good agreement'. For analyses of changes in the regionally averaged variables, we used a two-sample Kolmogorov–Smirnov test.

3. Results

3.1. Model validation

When compared to observations (Harris *et al* 2020, Schneider *et al* 2020), all models broadly reproduce the seasonal distribution of precipitation over the Central Plains, including the annual peak in late spring (May–June) and the driest conditions during late fall and winter (November–February) (supplemental figure 1). For some models (e.g. ACCESS-ESM1-5, CanESM5) the seasonal precipitation peak is concentrated in one instead of two months, while in other models the peak precipitation is more broadly distributed across the warm season (e.g. GISS-E2-1-G). Most models also have a wet bias in precipitation compared to the observations, especially during the cold season.

Ridge indices in all the models are strongly correlated (1850–2020) with Central Plains MJJ precipitation, MJJ soil moisture, and the April–July drying index (supplemental figure 2). Correlations with precipitation and soil moisture are negative, consistent with the reconstructions and indicating higher values of the ridge index are associated with drier overall conditions. The April–July ridging index positively correlates with April–July drying, indicating a more rapid seasonal dry down during ridging events. Model ridge index correlations with precipitation (multi-model median $r = -0.59$) are stronger compared to soil moisture (multi-model median $r = -0.42$), and the model soil moisture correlations

are slightly weaker compared to the empirical indices ($r = -0.50$). This likely reflects the high level of tuning in generating the observational ridging and soil moisture indices and structural differences across the models, especially in the land surface. The drying effect of anomalous ridging in the models is also reflected when distributions of precipitation, soil moisture, and drying index anomalies are compared across major ridge and trough events during the 1851–1950 baseline period (supplemental figure 3). From these analyses, we conclude that model responses are consistent with the empirically identified relationship between ridging and soil moisture in the reconstructions.

3.2. Ensemble mean responses

The largest and most robust precipitation response in the model projections is the increase over the northern part of the Central Plains during February–March–April (FMA) (figure 2, left column). Precipitation in the south declines in some models during these months, but the stippling indicates this reduction is non-robust over most grid cells. Precipitation responses are mixed during MJJ (figure 2, center column), with four models (ACCESS-ESM1-5, CanESM5, EC-Earth3, IPSL-CM6A-LR) showing some robust increases in small areas of the Central Plains and only one model (MPI-ESM1-2-LR) with limited robust declines. By contrast, changes in vapor pressure deficit during MJJ (figure 2, right column) are large and robust across all models and the entire Central Plains region, reflecting the strong response of this variable to higher temperatures.

Ensemble mean changes in MJJ soil moisture are more robust and widespread compared to the precipitation responses (figure 3), with four of the six models (CanESM5, EC-Earth3, GISS-E2-1-G, MPI-ESM1-2-LR) projecting robust soil moisture declines by the end of the 21st century over substantial areas of the Central Plains. Responses in the other two models (ACCESS-ESM1-5, IPSL-CM6A-LR) are non-robust across most grid cells in the Central Plains. The stronger responses in soil moisture compared to precipitation are likely a consequence of the much stronger increases in evaporative demand that are driven, at least in part, by the increases in vapor pressure deficit.

3.3. Regional average shifts in drought and ridging

Regional average distributions of Central Plains MJJ precipitation, MJJ vapor pressure deficit, MJJ soil moisture, April–July drying index, and the MJJ ridge index are shown for three time periods (1851–1950, 1985–2014, 2071–2100) in figure 4. The colored dots indicate models where the 2071–2100 distributions are significantly different (two-sample Kolmogorov–Smirnov test, $p \leqslant 0.05$) from 1851–1950 (blue squares) or 1985–2014 (brown circles). Averaged over the Central Plains region, most models experience significant increases in MJJ precipitation by the end of the 21st century (figure 4(a)). MPI-ESM1-2-LR is the only model to show significant declines, and responses in GISS-E2-1-G are insignificant. By contrast, all models show large and significant increases in vapor pressure deficit by the end of the 21st century (figure 4(b)).

Despite the absence of any large-scale declines in either FMA or MJJ precipitation over the Central Plains, soil moisture decreases in all models except ACCESS-ESM1-5 by the end of the 21st century (figure 4(c)). In CanESM5, EC-Earth3, and MPI-ESM1-2-LR, 2071–2100 soil moisture is significantly lower when compared to both the baseline and the end of the historical simulations. Soil moisture is significantly drier in IPSL-CM6A-LR when compared to 1851–1950 but not 1985–2014 because most of the total decline has already occurred by the early 21st century. Soil moisture in GISS-E2-1-G actually increases from the baseline period to the end of the historical simulation, with significant declines only occurring afterwards. This transient response is likely a consequence of the inclusion of irrigation in the GISS-E2-1-G simulations as an anthropogenic forcing (Miller *et al* 2021). Irrigation rates in GISS-E2-1-G increase steadily over the course of the historical simulation (Cook *et al* 2020), with this additional flux of water compensating for the warming induced soil moisture decline over the Central Plains at the beginning of the 21st century (Cook *et al* 2019, 2020). For the projections, however, irrigation inputs remain fixed at early twenty-first century values out to 2100, even as greenhouse gas forcing and temperatures continue to increase. By the end of the 21st century, these fixed irrigation rates are no longer sufficient to counteract the enhanced soil moisture drying at these higher warming levels. To our knowledge, none of the other models we analyzed included irrigation in their CMIP6 model simulations.

All models show significant increases in the April–July drying index for 2071–2100 (figure 4(d)), including ACCESS-ESM1-5, a model where total MJJ soil moisture changes are insignificant, and GISS-E2-1-G, which includes the transient irrigation forcing. This is indicative of a more rapid seasonal drawdown of soil moisture during the transition period into the warmest and most moisture stressed months of the year. As with the overall drying evidenced in the models, the most likely driver is the robust increase in vapor pressure deficit and evaporative demand in the atmosphere. These results suggest that, even in models where precipitation increases and mean state soil moisture changes during MJJ are negligible, there will

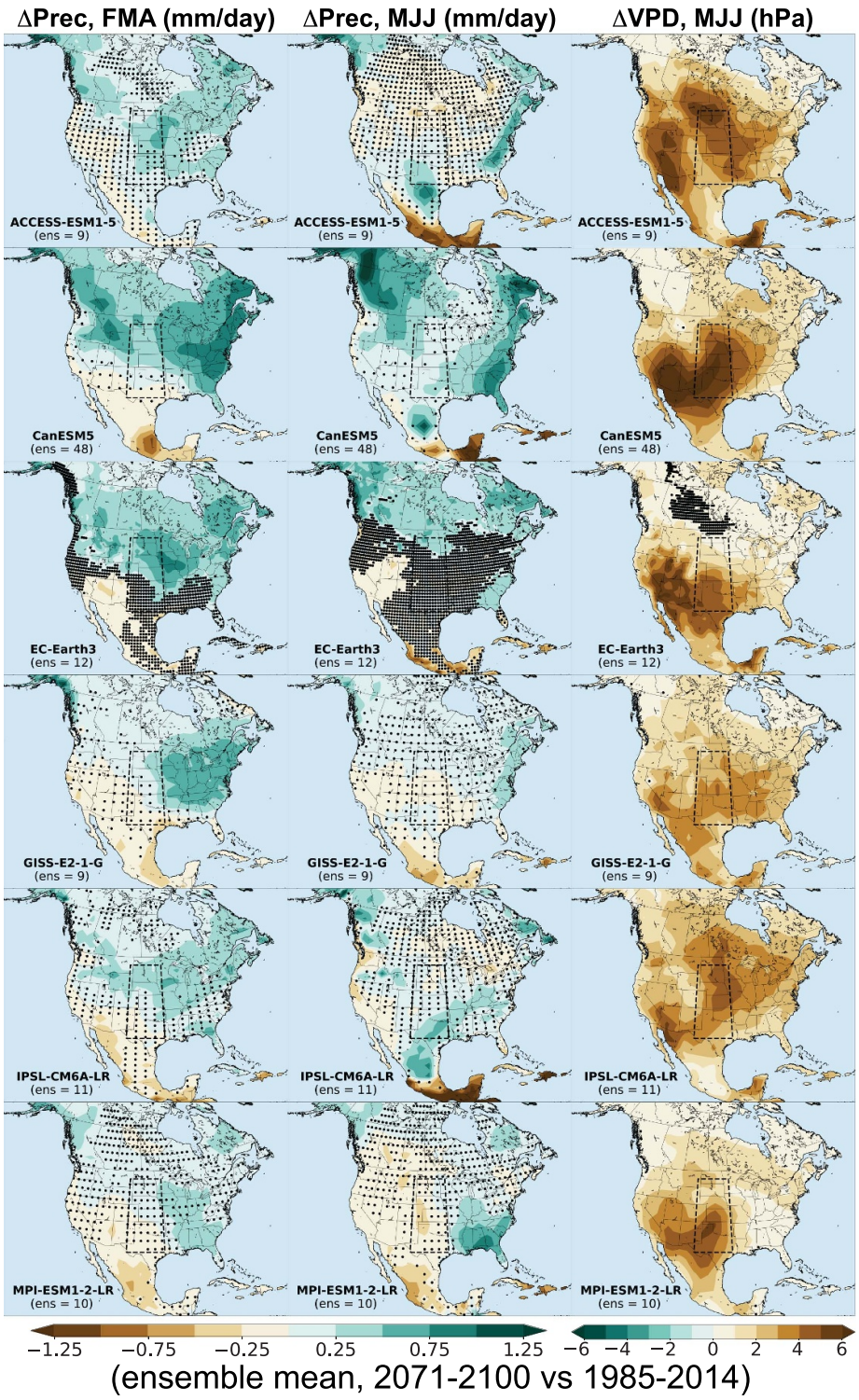

Figure 2. Seasonal changes (2071–2100 vs 1985–2014, SSP2-4.5 scenario) in ensemble mean precipitation (February–March–April, FMA; May–June–July, MJJ) and vapor pressure deficit (MJJ). Dashed black box outlines the Central Plains region (32–47° N, 105–95° W) used for regional averaging. Stippling indicates grid cells with non-robust responses ($R < 0.80$).

likely still be some increase in drought stress from peak spring (April) into peak summer (July). Finally, four models (figure 4(e)) show significant increases in the ridge index, with insignificant changes in GISS-E2-1-G and declines in the ridge index in ACCESS-ESM1-5.

3.4. The effect of ridge events in a warmer world

To better understand how the effects of ridging on Central Plains drought change with warming, we compiled MJJ precipitation, MJJ vapor pressure deficit, MJJ soil moisture, and the April–July drying index during major ridge events for our three time

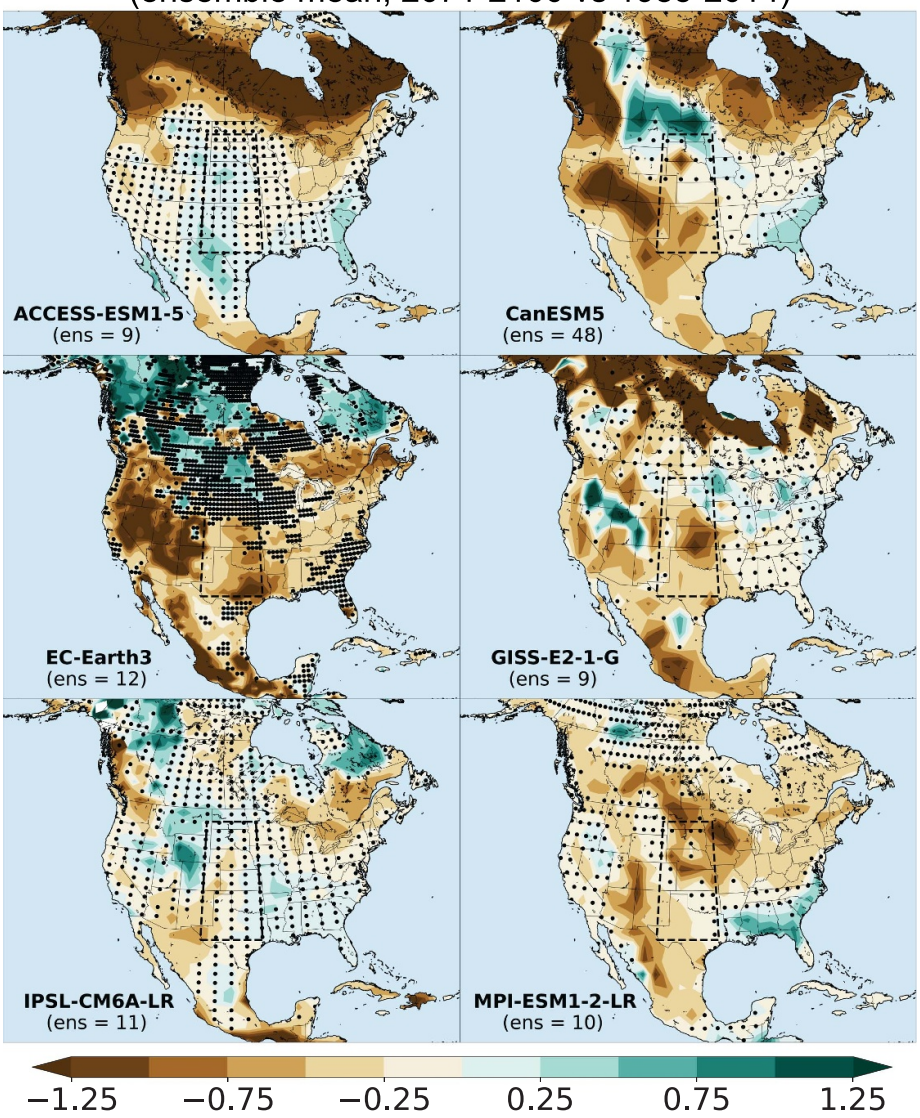

Figure 3. Changes (2071–2100 vs 1985–2014, SSP2-4.5 scenario) in ensemble mean 0–200 cm standardized soil moisture (unit standard deviation) during May–June–July (MJJ). Dashed black box outlines the Central Plains region (32–47° N, 105–95° W) used for regional averaging. Stippling indicates grid cells with non-robust responses ($R < 0.80$).

periods of interest (1851–1950, 1985–2014, 2071–2100) (figure 5). Consistent with the analyses of the empirical indices (figure 1(c)), major ridge events are defined as years where the ridge index falls within the upper quartile, with this threshold calculated for each model separately using the 1851–1950 baseline period. As in figure 4, blue squares and brown circles indicate where the 2071–2100 distributions are significantly different from the 1851–1950 and 1985–2014 intervals.

For most models, changes in precipitation (figure 5(a)) and vapor pressure deficit (figure 5(b)) during ridging events largely reflect the mean or median shifts of these variables in the models. For example, precipitation increases during ridging events at the end of the 21st century in CanESM5, EC-Earth3, and IPSL-CM6A-LR, all models that show significant increases in precipitation (figure 4(a)). Similarly, precipitation deficits during ridge events are amplified in MPI-ESM1-2-LR, the one model with a significant decline in precipitation. The exception is ACCESS-ESM1-5, where precipitation deficits are much larger during ridge events, despite an overall shift towards increased precipitation. This change is insignificant, however, and may reflect the limited number of major ridge events (only 11) available from this model during 2071–2100. Consistent with the robust increase in vapor pressure deficit in all models, vapor pressure deficit during ridging events significantly increases in all models.

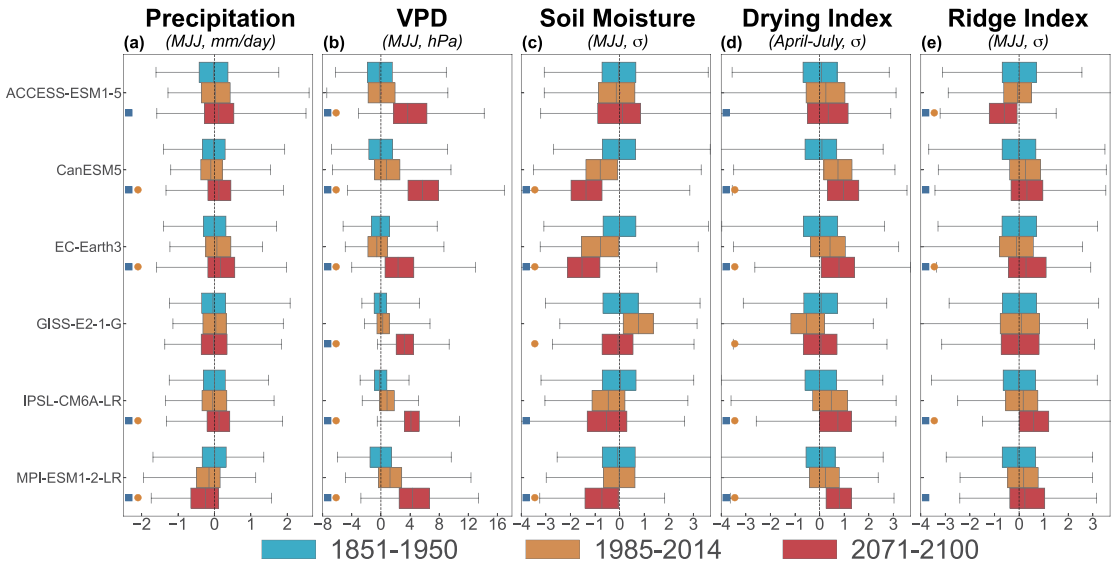

Figure 4. Regional average anomalies from the CMIP6 ensembles over the Central Plains (32–47° N, 105–95° W): (a) May–June–July (MJJ) precipitation, (b) MJJ vapor pressure deficit (VPD), (c) MJJ 0–200 cm soil moisture, (d) April–July the drying index, and (e) the MJJ ridge index. Each box plot contains all years from all ensemble members for the indicated time periods. Blue squares indicate significant (two-sided Kolmogorov–Smirnov test, $p \leqslant 0.05$) shifts in the distribution between 2071–2100 and our baseline period (1851–1950). Brown circles indicate significant shifts in the distribution between 2071–2100 and the last 30 years of the historical simulation (1985).

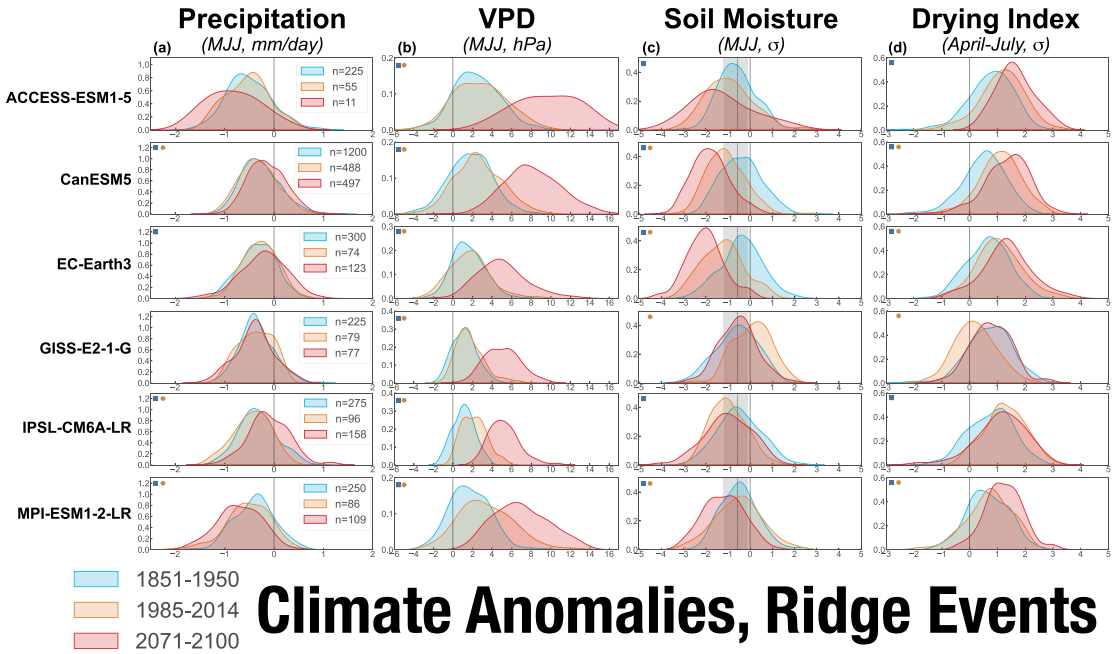

Figure 5. Distributions (kernel density plots) of (a) May–June–July (MJJ) precipitation, (b) MJJ vapor pressure deficit (VPD), (c) MJJ soil moisture, and (d) April–July drying index from the CMIP6 ensembles for the Central Plains (32–47° N, 105–95° W) during major ridge events. Major ridge events are defined as years where the ridging index falls within the upper quartile, defined using the baseline period (1851–1950). Each distribution contains all years from all ensemble members for the indicated time periods. Blue squares indicate significant (two-sided Kolmogorov–Smirnov test, $p \leqslant 0.05$) shifts in the distribution between 2071–2100 and our baseline period (1851–1950). Brown circles indicate significant shifts in the distribution between 2071–2100 and the last 30 years of the historical simulation (1985–2014). Gray shading and vertical dashed black lines in the soil moisture plots are the interquartile range and the median from the soil moisture reconstruction (1500–2020), respectively.

All models indicate that ridge events in the future will have significantly reduced soil moisture (figure 5(c)) and more rapid seasonal soil moisture declines (figure 5(d)). Notably, the enhanced surface drying effect of the ridges even occurs in models with median precipitation increases (e.g. CanESM5, EC-Earth3) or negligible changes in mean soil moisture (ACCESS-ESM1-5). This further supports a critical role for increased evaporative demand in projected soil moisture dynamics over the region and suggests

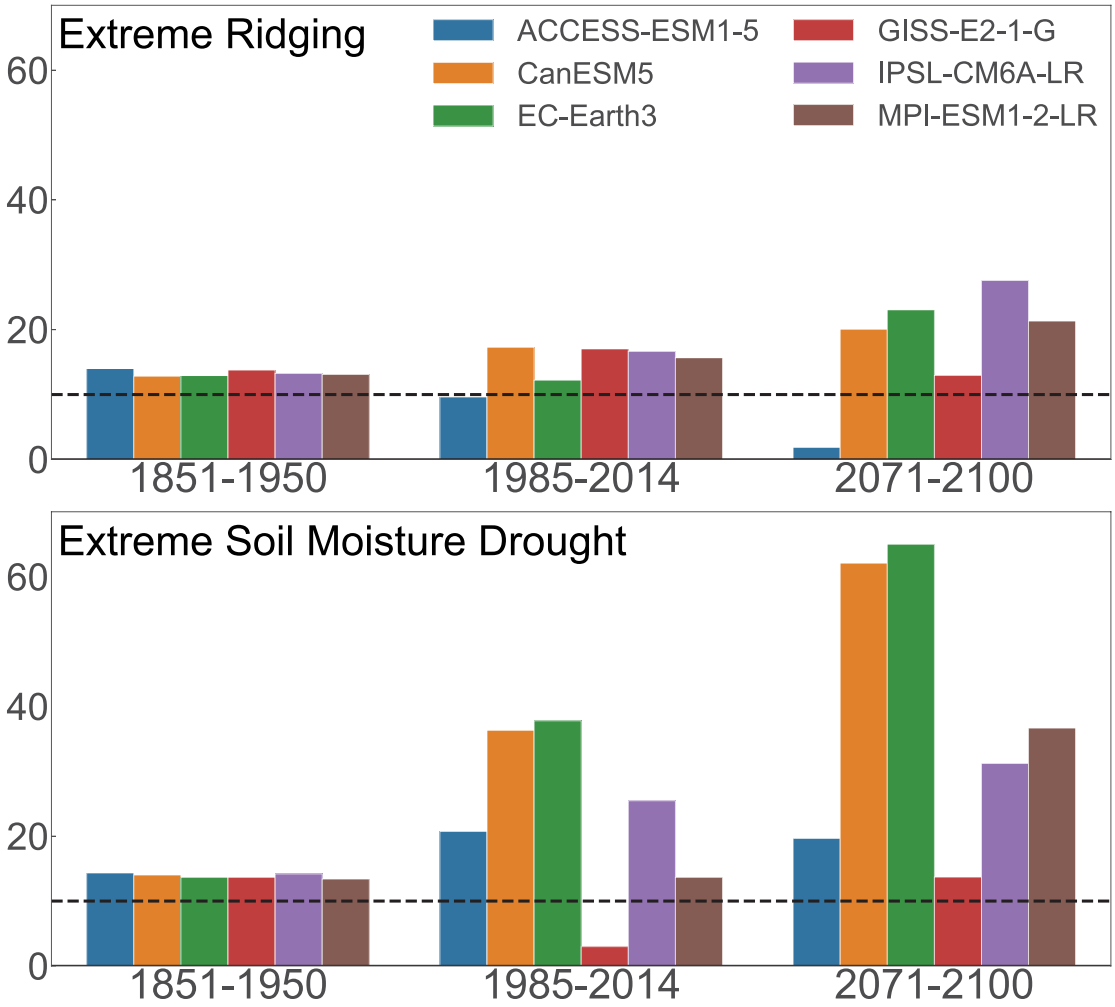

Figure 6. Risk or likelihood (%) of extreme ridge or soil moisture drought events during different intervals in the CMIP6 ensembles. Extreme ridge events are defined as years in the models where the ridge index meets or exceeds the 90th percentile from the full ridge index reconstruction (1500–2020). Extreme drought events are defined as years in the models where soil moisture is below the 10th percentile from the full empirical soil moisture index (1500–2020).

that, even in a scenario where mean conditions do not significantly change, a warmer world has the potential to still amplify drought events (e.g. caused by a major ridge) when they do occur.

3.5. Extreme ridge and drought events

As a consequence of the mean hydroclimate shifts and the amplified effect of ridging on drought, the Central Plains is likely to experience a substantial increase in the risk of the most severe ridge events and droughts observed over the last 500 years. We define these extreme events as years in the different ensembles where the magnitude of the ridge or soil moisture indices fall within the upper or lower tenth percentile calculated across the entire period covered by the reconstruction and observations (1500–2020; dashed lines in figure 6). Event risk for the different models and time periods is then calculated as the proportion of years from the entire ensemble that exceed these thresholds. Risk values $> 10\%$ indicate a higher likelihood of these events in the models compared to the reconstructions, while values $< 10\%$ indicate a reduced risk.

For the baseline period in the models (1851–1950), extreme event risk for ridges and droughts is slightly higher compared to the reconstructions (figure 6). In later periods, the risk of extreme ridges increases in all models except ACCESS-ESM1-5 (figure 6, top panel), though these changes are relatively modest. Most models show much larger increases in extreme drought risk, including models where the median climate is not significantly drying (e.g. ACCESS-ESM1-5) (figure 6, bottom panel). By the end of the 21st century, extreme drought risk in every model exceeds the baseline risk in the reconstruction, and all models except GISS-E2-1-G have higher risk when compared to the 1851–1950 baseline. At the most extreme end, CanESM5 and

EC-Earth3 both experience a $>60\%$ likelihood of these extreme droughts occurring in 2071–2100, a six-fold increase compared to the reconstruction. In aggregate, the multi-model median extreme drought risk for 2071–2100 is 33.9%, 3× the risk from the reconstruction and a 2.5× increase over the multi-model median from the baseline period (1851–1950).

4. Discussion and conclusions

Our analyses of six CMIP6 climate model ensembles highlight how, in spite of uncertain changes in precipitation, early summer soil moisture drought over the Central Plains is likely to increase in frequency and severity under a moderate warming scenario. Further, even in models where changes in mean state soil moisture are insignificant, the drying effect of atmospheric ridging events on soil moisture drought will likely be intensified. While most models show some increase in the ridging index, the increases in soil moisture drought severity and risk appear most strongly connected to warming induced increases in vapor pressure deficit and evaporative demand. In aggregate, these models project a three-fold increase in the risk of severe droughts over the Central Plains, events that are analogous to the worst droughts of the last 500 years.

These results are largely consistent with analyses using the previous (Cook *et al* 2015, Feng *et al* 2017) and current (Cook *et al* 2020, Marvel *et al* 2021) generations of climate models. One weakness in our approach, however, is the limited number of models that were able to provide the necessary diagnostic output for our calculations. First, it is unclear if these six models adequately cover the range of structural uncertainties that could be important for drought projections in the region, especially at the land surface. Vegetation, for example, strongly modulates surface moisture partitioning, especially evapotranspiration, and changes in climate and atmospheric carbon dioxide concentrations can affect vegetation in ways that diminish (Swann 2018) or amplify (Mankin *et al* 2019) evaporative losses and soil moisture drying. Second, it is unclear how well the multi-model ensemble encompasses the full range of projected precipitation responses. While the soil moisture declines appear driven primarily by increased evaporative demand, other studies have demonstrated the importance of changes in mean precipitation and precipitation variability for interpretations of drought in climate model projections (Ukkola *et al* 2020, Cook *et al* 2021).

We also note that the correlations between soil moisture and the ridging index in the models were weaker when compared to the reconstructions. This may be partially a consequence of how the empirical soil moisture and ridge indices were developed by Bolles *et al* (2021), who selected variables over regions designed to maximize the correlation between the soil moisture and ridge indices. While we used the same definitions when constructing the same indices in the models for consistency, alternative approaches more tightly tuned to the individual models could result in stronger correlations. Additionally, the large area representing the Central Plains in this study and Bolles *et al* (2021) may conflate seasonal precipitation dynamics and drought responses that differ substantially between the northern and southern parts of this region (Cook *et al* 2020, Ukkola *et al* 2020, Marvel *et al* 2021). Analyses more focused on small regions, in addition to model-based development of the soil moisture and ridging indices, could therefore potentially generate different insights.

The Central Plains region has experienced severe drought events in the recent (Schubert *et al* 2004b, Hoerling *et al* 2014) and distant (Woodhouse and Overpeck 1998) past, and the IPCC AR6 projects an increase in soil moisture drought in the region if global temperatures exceed 2 °C above pre-industrial levels (Seneviratne *et al* 2021). Our results support this conclusion, but what is more uncertain are the consequences of these increases in drought severity and risk. The Central Plains is a critically important region for agriculture, ecosystem services, and natural resources (Ojima *et al* 2021). Agriculture, in particular, has benefited significantly from management practices that have increased drought resiliency in the region, including irrigation (Evett *et al* 2020) and improved soil conservation practices (Lee and Gill 2015). While these systems have been effective for reducing drought impacts during recent single-year droughts (e.g. 2012), much of the region has not experienced an extended drought event since the Dust Bowl of the 1930s. It's therefore unclear how effective current measures will be in a future with drought events that are more severe and hotter than similar events in the past.

Finally, we note that the approach we have taken in this study, where we analyzed drought during specified circulation anomalies under different warming levels, could easily be applied and informative for other regions and extreme events. Most climate extremes are associated with large-scale, often intense and persistent atmospheric circulation patterns (Seager *et al* 2015, Tomczyk and Bednorz 2016, Breugem *et al* 2020, Kautz *et al* 2022, White *et al* 2022). But even while atmospheric circulation responses to warming remain highly uncertain (Li *et al* 2018, Huguenin *et al* 2020), circulation variability itself will still play a critical role in the occurrence of climate extremes in the future (Mankin *et al* 2020). Our results demonstrate that the same circulation regime in a warmer future may lead to more intense or frequent extremes events compared to the past. Studies of these circulation events under different warming levels may therefore

provide important information on the potentially changing role of circulation in various aspects of climate extremes, beyond basic analyses of mean state changes.

Data availability statement

Climate model data that support the findings of this study are openly available at the following URL/DOI: https://esgf-node.llnl.gov/search/cmip6/. Observed and reconstructed ridge and soil moisture indiced can be found at the following URL/DOI: www.dropbox.com/s/yv3hbioaid0bcko/reconstructions_stand.csv.

Acknowledgments

This work was supported by NOAA MAPP NA19OAR4310278 (B I C, A P W, K M) and NASA's Modeling, Analysis, and Prediction program (B I C, A P W).

Conflict of interest

The authors declare no competing interests.

References

Basara J B, Christian J I, Wakefield R A, Otkin J A, Hunt E H and Brown D P 2019 *Environ. Res. Lett.* **14** 084025
Basara J B, Maybourn J N, Peirano C M, Tate J E, Brown P J, Hoey J D and Smith B R 2013 **4** 72–81
Bolles K C, Williams A P, Cook E R, Cook B I and Bishop D A 2021 *Geophys. Res. Lett.* **48** e2020GL091271
Boucher O, Denvil S, Caubel A and Foujols M A 2018 IPSL IPSL-CM6A-LR model output prepared for CMIP6 CMIP (https://doi.org/10.22033/ESGF/CMIP6.1534)
Boucher O, Denvil S, Caubel A and Foujols M A 2019 IPSL IPSL-CM6A-LR model output prepared for CMIP6 ScenarioMIP (https://doi.org/10.22033/ESGF/CMIP6.1532)
Breugem A J, Wesseling J G, Oostindie K and Ritsema C J 2020 *Earth-Sci. Rev.* **204** 103171
Cook B I, Ault T R and Smerdon J E 2015 *Sci. Adv.* **1** e1400082
Cook B I, Mankin J S, Marvel K, Williams A P, Smerdon J E and Anchukaitis K J 2020 *Earth's Future* **8** e2019EF001461
Cook B I, Mankin J S, Williams A P, Marvel K D, Smerdon J E and Liu H 2021 *Earth's Future* **9** e2021EF002014
Cook B I, McDermid S S, Puma M J, Williams A P, Seager R, Kelley M, Nazarenko L and Aleinov I 2020 *J. Geophys. Res.* **125** e2019JD031814
Cook B I, Miller R L and Seager R 2009 *Proc. Natl Acad. Sci.* **106** 4997–5001
Cook B I, Seager R and Smerdon J E 2014 *Geophys. Res. Lett.* **41** 7298–305
Cook B I, Seager R, Williams A P, Puma M J, McDermid S, Kelley M and Nazarenko L 2019 *J. Clim.* **32** 5417–36
Coumou D, Di Capua G, Vavrus S, Wang L and Wang S 2018 *Nat. Commun.* **9** 2959
Cowan T, Hegerl G C, Schurer A, Tett S F B, Vautard R, Yiou P, Jézéquel A, Otto F E L, Harrington L J and Ng B 2020 *Nat. Commun.* **11** 2870
Dong X *et al* 2011 *J. Geophys. Res.* **116** D03204
EC-Earth Consortium 2019a EC-Earth-Consortium EC-Earth3 model output prepared for CMIP6 CMIP historical (https://doi.org/10.22033/ESGF/CMIP6.4700)
EC-Earth Consortium 2019b EC-Earth-Consortium EC-Earth3-Veg model output prepared for CMIP6 ScenarioMIP (https://doi.org/10.22033/ESGF/CMIP6.727)
Evett S R, Colaizzi P D, Lamm F R, O'Shaughnessy S A, Heeren D M, Trout T J, Kranz W L and Lin X 2020 *Trans. ASABE* **63** 703–29
Eyring V, Bony S, Meehl G A, Senior C, Stevens B, Stouffer R J and Taylor K E 2016 *Geosci. Model Dev. Discuss.* **8** 1937–58
Feng S, Trnka M, Hayes M and Zhang Y 2017 *J. Clim.* **30** 265–78
Harris I, Osborn T J, Jones P and Lister D 2020 *Sci. Data* **7** 109
Hausfather Z, Marvel K, Schmidt G A, Nielsen-Gammon J W and Zelinka M 2022 *Nature* **605** 26–29
Heim R R 2017 *Bull. Am. Meteorol. Soc.* **98** 2579–92
Hobbins M T, Wood A, McEvoy D J, Huntington J L, Morton C, Anderson M and Hain C 2016 *J. Hydrometeorol.* **17** 1745–61
Hoerling M, Eischeid J, Kumar A, Leung R, Mariotti A, Mo K, Schubert S and Seager R 2014 *Bull. Am. Meteorol. Soc.* **95** 269–82
Huguenin M F, Fischer E M, Kotlarski S, Scherrer S C, Schwierz C and Knutti R 2020 *Geophys. Res. Lett.* **47** e2019GL086132
Jong B T, Newman M and Hoell A 2022 *J. Clim.* **35** 2525–47
Kautz L A, Martius O, Pfahl S, Pinto J G, Ramos A M, Sousa P M and Woollings T 2022 *Weather Clim. Dyn.* **3** 305–36
Knutti R and Sedlacek J 2013 *Nat. Clim. Change* **3** 369–73
Kornhuber K and Tamarin-Brodsky T 2021 *Geophys. Res. Lett.* **48** e2020GL091603
Lawrence M G 2005 *Bull. Am. Meteorol. Soc.* **86** 225–34
Lee J A and Gill T E 2015 *Aeolian Res.* **19** 15–36
Li C *et al* 2018 *Earth Syst. Dyn.* **9** 359–82
Logan K, Brunsell N, Jones A and Feddema J 2010 *J. Arid Environ.* **74** 247–55
Mankin J S, Lehner F, Coats S and McKinnon K A 2020 *Earth's Future* **8** e2012EF001610
Mankin J S, Seager R, Smerdon J E, Cook B I and Williams A P 2019 *Nat. Geosci.* **12** 983–8
Marvel K, Cook B I, Bonfils C, Smerdon J E, Williams A P and Liu H 2021 *Earth's Future* **9** e2021EF002019
Meehl G A, Senior C A, Eyring V, Flato G, Lamarque J F, Stouffer R J, Taylor K E and Schlund M 2020 *Sci. Adv.* **6** eaba1981
Miller R L *et al* 2021 *J. Adv. Model. Earth Syst.* **13** e2019MS002034
NASA GISS 2018 NASA-GISS GISS-E2.1G model output prepared for CMIP6 CMIP (https://doi.org/10.22033/ESGF/CMIP6.1400)
NASA GISS 2020 NASA-GISS GISS-E2.1G model output prepared for CMIP6 ScenarioMIP (https://doi.org/10.22033/ESGF/CMIP6.2074)
Ojima D S, Conant R T, Parton W, Lackett J M and Even T L 2021 *Rangel. Ecol. Manage.* **78** 180–90
Otkin J A, Anderson M C, Hain C, Svoboda M, Johnson D, Mueller R, Tadesse T, Wardlow B and Brown J 2016 *Agric. For. Meteorol.* **218-219** 230–42
Otkin J A, Svoboda M, Hunt E D, Ford T W, Anderson M C, Hain C and Basara J B 2018 *Bull. Am. Meteorol. Soc.* **99** 911–9
Palmer W C and Seamon L H 1957 *Weatherwise* **10** 22–25
Pendergrass A G *et al* 2020 *Nat. Clim. Change* **10** 191–9
Schneider U, Becker A, Finger P, Rustemeier E and Ziese M 2020 *Global Precipitation Climatology Centre (GPCC) at Deutscher Wetterdienst*
Schubert S D, Suarez M J, Pegion P J, Koster R D and Bacmeister J T 2004a *J. Clim.* **17** 485–503
Schubert S D, Suarez M J, Pegion P J, Koster R D and Bacmeister J T 2004b *Science* **303** 1855–9
Seager R, Hoerling M, Schubert S, Wang H, Lyon B, Kumar A, Nakamura J and Henderson N 2015 *J. Clim.* **28** 6997–7024
Seneviratne S I *et al* 2021 Weather and climate extreme events in a changing climate *Climate Change 2021: The Physical Science Basis. Contribution of Working Group I to the Sixth Assessment Report of the Intergovernmental Panel on Climate Change* (Cambridge: Cambridge University Press)
Sherwood S C *et al* 2020 *Rev. Geophys.* **58** e2019RG000678

Sun X, Ding Q, Wang S Y S, Topál D, Li Q, Castro C, Teng H, Luo R and Ding Y 2022 *Nat. Commun.* **13** 1288
Swann A L S 2018 *Curr. Clim. Change Rep.* **4** 192–201
Swart N C *et al* 2019a CCCma CanESM5 model output prepared for CMIP6 CMIP historical (https://doi.org/10.22033/ESGF/CMIP6.3610)
Swart N C *et al* 2019b CCCma CanESM5 model output prepared for CMIP6 ScenarioMIP (https://doi.org/10.22033/ESGF/CMIP6.1317)
Ting M, Seager R, Li C, Liu H and Henderson N 2021 *J. Clim.* **34** 9043–56
Tomczyk A M and Bednorz E 2016 *Int. J. Climatol.* **36** 770–82
Trenberth K E, Branstator G W and Arkin P A 1988 *Science* **242** 1640–5
Ukkola A M, De Kauwe M G, Roderick M L, Abramowitz G and Pitman A J 2020 *Geophys. Res. Lett.* **47** e2020GL087820
Wang S Y S *et al* 2015 *J. Geophys. Res.* **120** 8804–16
White R H, Kornhuber K, Martius O and Wirth V 2022 *Bull. Am. Meteorol. Soc.* **103** E923–35
Wieners K-H *et al* 2019a MPI-M MPIESM1.2-LR model output prepared for CMIP6 CMIP (https://doi.org/10.22033/ESGF/CMIP6.742)
Wieners K-H *et al* 2019b MPI-M MPIESM1.2-LR model output prepared for CMIP6 ScenarioMIP (https://doi.org/10.22033/ESGF/CMIP6.793)
Woodhouse C A and Overpeck J T 1998 *Bull. Am. Meteorol. Soc.* **79** 2693–714
Ziehn T *et al* 2019a CSIRO ACCESS-ESM1.5 model output prepared for CMIP6 CMIP (https://doi.org/10.22033/ESGF/CMIP6.2288)
Ziehn T *et al* 2019b CSIRO ACCESS-ESM1.5 model output prepared for CMIP6 ScenarioMIP (https://doi.org/10.22033/ESGF/CMIP6.2291)